SCIENCE CHINA Materials ARTICLES

mater.scichina.com link.springer.com

Published online 1 February 2021 | https://doi.org/10.1007/s40843-020-1560-1
Sci China Mater 2021, 64(7): 1713–1722

Electron configurations at 3d orbital of metal ion determining charge transition process in memory devices

Jiacong Guo[1], Yankun Zhang[1], Guofeng Tian[1], Deyang Ji[2,3*], Shengli Qi[1,4*], Dezhen Wu[1,4] and Wenping Hu[5]

ABSTRACT **Functional polymeric materials with electrical bi-stable states possess significant potential for high-density data storage due to their nanoscale memory site, three-dimensional-stacking ability and intrinsic flexibility. Aromatic polyimides bearing donor-acceptor (D-A) skeleton could form the charge transfer complex (CTC) under an electrical field, leading to their feasibility as memory materials. Three novel porphyrinated polyimides DATPP-DSDA, Zn-DATPP-DSDA and Mn-DATPP-DSDA were designed and synthesized for information memory applications. Metal ions with different electron configurations at 3d orbital have a determining influence on memory behaviors of polyimides: nonvolatile write-once-read-many-times memory (WORM) for DATPP-DSDA, volatile static random access memory (SRAM) for Zn-DATPP-DSDA, but no memory performance for Mn-DATPP-DSDA. By comparing the contribution of orbital transition and hole-electron distribution of charge-transfer excited states, roles of metal ions in regulating memory types were discussed. Molecular simulation results indicate that the Zn ion could play a bridge role in paving the route for excited electrons from a D to an A, while a trap role for the Mn ion in hindering this process. This study proves the feasibility of the strategy for modulating the memory behaviors of porphyrinated polyimides by varying the central metal ion and provides the exact effects of various metal ions on regulating charge transfer processes.**

Keywords: memory, polyimide, porphyrin, charge transfer

INTRODUCTION

Polymeric materials are considered as substitutes for traditional silicon-based memory materials because of their prominent advantages including flexibility, low cost, large memory capacity and simple manufacturing process [1–4]. Among a variety of polymeric materials, aromatic polyimides (PIs) with electron donor-acceptor (D-A) structures show great potential for memory applications due to their low expansion coefficient, simple synthesis process and excellent chemical/thermal stability [5–8]. Generally, this kind of PIs could form the charge transfer complex (CTC) under a suitable applied electric field, which could provide low (OFF) and high (ON) conductivity states for information memory applications. In last decade, different kinds of memory behaviors based on PIs have been reported, such as volatile dynamic random access memory (DRAM) [6,9–11], volatile static random access memory (SRAM) [12–14], nonvolatile flash [15–17] and write-once-read-many-times memory (WORM) [18–20]. It is worth noting that organic materials containing various metal ions for memory applications have been studied; however, most of the research is focused on ferrocene [21–23], different functional groups attaching to ligand [24–25] or complex containing only one kind of metal [26–28]. Furthermore, the mechanism of metal ions controlling memory performances is still not clear.

[1] State Key Laboratory of Chemical Resource Engineering, Beijing University of Chemical Technology, Beijing 100029, China
[2] Tianjin Key Laboratory of Molecular Optoelectronic Science, Department of Chemistry, Institute of Molecular Aggregation Science, Tianjin University, Tianjin 300072, China
[3] Beijing National Laboratory for Molecular Sciences, Beijing 100190, China
[4] Changzhou Institute of Advanced Materials, Beijing University of Chemical Technology, Changzhou 213164, China
[5] Tianjin Key Laboratory of Molecular Optoelectronic Science, Department of Chemistry, School of Science, Tianjin University & Collaborative Innovation Center of Chemical Science and Engineering, Tianjin 300072, China
* Corresponding authors (emails: jideyang@tju.edu.cn (Ji D); qisl@mail.buct.edu.cn (Qi S))

Porphyrins, a class of organic macrocyclic substances with electron donor characteristic, possess 26 delocalized electrons and bear co-planar conjugated structure. The core position of porphyrin ring provides the ability to complex up to 56 different metal elements [29], and its electronic structure could be regulated by simply varying the central metal ion to achieve expected functions. For example, the capacity of the zinc (Zn) ion to raise the electronic density of porphyrin ring endows the Zn porphyrins with the applications for solar cells [30–32] and organic light emitting diodes (OLEDs) [33–35]. The high spin state and coordination effect of the manganese (Mn) ion make Mn porphyrins widely used in simulation of cytochrome P450 [36–38] and sensors [39–41]. As a matter of fact, all the above-mentioned applications could be attributed to metal ions with various electron configurations at 3d orbital. Therefore, the donor feature and variable applications in optics and electronics provide an ideal platform to further investigate the mechanism of metal ions for memory behaviors and clarify the moderation effect of metal ions with various electron configurations. Though pioneer zinc-porphyrin based memory PIs and corresponding effects of Zn ions have been reported and proposed [42–43], the exact role of Zn ions in tailoring memory behaviors is not so precise and still not proved by experimental or theoretical results, which requires deeper and more accurate investigation.

In this study, three novel porphyrinated PIs abbreviated as DATPP-DSDA, Zn-DATPP-DSDA and Mn-DATPP-DSDA were designed and synthesized as active memory materials. Molecular simulation results indicate that these two kinds of metal ions make different contributions to the regulation of charge transfer in porphyrinated PIs. Because of its orbital features, the Zn ion acts as a bridge paving the path for electrons to migrate between D and A moieties, while the Mn ion functions as a trap to impede this process. Simultaneously, experimental results further demonstrate that DATPP-DSDA-based memory devices show non-volatile WORM memory behavior. With insertion of a zinc ion into the core of porphyrin ring, Zn-DATPP-DSDA provides volatile SRAM memory performance. Expectedly, Mn-DATPP-DSDA, without the electrical bistable states, possesses no memory performances. The variable memory behaviors are consistent with molecular simulation and prove the feasibility of regulating memory performances by controlling the metal ions. This study not only offers a basis for the selection of ideal electronic structure of metal ions in the porphyrin ring but also provides theoretical guidance for the application of porphyrin in optoelectronics.

EXPERIMENTAL SECTION

Materials

Tetraphenylporphyrin (TPP) was purchased from Energy Chemical. 3,3′,4,4′-diphenylsulfone tetracarboxylic dianhydride (DSDA) was purchased from Tokyo Chemical Industry. Zinc acetate and manganese acetate were purchased from Bide Pharmatech Ltd. Isoquinoline and *m*-cresol were purchased from J&K Scientific. Other solvents and reagents were purchased from Beijing Chemical Works. *m*-Cresol were distilled before use. Other chemicals were used without further purification.

Instruments and measurements

^{1}H-nuclear magnetic resonance (NMR) spectra of the synthesized compounds were measured on a Bruker AV400 spectrometer. Fourier transform infrared (FT-IR) spectra of the synthesized compounds on KBr substrate were tested under ambient conditions using a Bruker Tensor infrared spectrophotometer. Elemental analysis was analyzed on a varioELcube elemental analyzer. The X-ray diffraction (XRD) was measured with an UltimaIII X-ray diffractometer. The gel permeation chromatography (GPC) analysis was carried out on a Waters 515-2410 system using polystyrene standard as the molecular weight reference and *N*,*N*-dimethyl formamide (DMF) as the eluent. The film morphology and surface roughness were characterized by atomic force microscopy (AFM) with a Nanoscope 3D Controller in tapping mode. Ultraviolet-visible (UV-vis) absorption spectra were recorded on a Shimadzu UV-2550 spectrophotometer. Cyclic voltammograms (CV) were recorded on a CHI660D electrochemical Workstation (Shanghai Chenhua Instruments Inc. China) using a three-electrode cell under N_2 atmosphere. The PI coated on indium tin oxide (ITO) conductive glass acted as the working electrode and was scanned anodically and cathodically (scan rate: 100 mV s^{-1}) in a solution of tetrabutylammonium tetrafluoroborate (*n*-Bu_4BF_4) in dry acetonitrile (0.1 mol L^{-1}). Ag/AgCl electrode and platinum net acted as the reference electrode and the auxiliary electrode, respectively. Ferrocene was used as the external reference for calibration (0.38 V *vs.* Ag/AgCl). The electrical bistability and operation stability of the memories were characterized on a Keithley 4200 SCS semiconductor parameter analyzer

equipped with a Micromanipulator PW-600 probe station (Advanced Technology Co. Ltd, Hong Kong).

Synthesis of the porphyrinated polyimides *via* one-step process

Porphyrin-based diamine (DATPP) and its metal complex (M-DATPP, M = Zn or Mn) were synthesized, as shown in Scheme S1 and the corresponding results of structure characterization are given in Figs S1–S7. Three porphyrinated PIs, DATPP-DSDA, Zn-DATPP-DSDA and Mn-DATPP-DSDA were designed and synthesized *via* a typical one-step imidization process, as shown in Scheme S2. Taking DATPP-DSDA as an example, a solution of equimolar amounts of DATPP and DSDA was mixed and stirred vigorously in *m*-cresol at 50°C for 4 h followed by reacting with 0.5 mL of isoquinoline at 190°C for 12 h. The whole reaction process was conducted under inert N_2 atmosphere. Then the resulting mixture was cooled to room temperature and poured to 300 mL of methanol. The synthesized PIs were washed with methanol for several times and collected by filtration. Residual organic solvents were removed by heating in a vacuum oven at 80°C.

Fabrication of sandwiched devices

The memory devices were fabricated with the configuration of Al/PIs/ITO, where Al and ITO worked as top and ground electrodes, as shown in Fig. 1a. Firstly, the ITO substrate was successively cleaned with isopropanol, ethanol and chloroform by ultrasonication for 20 min. Then the PIs of 20 mg mL^{-1}, after being filtered through polytetrafluoroethylene membrane syringe filters with a pore size of 0.22 mm, was spin-coated on ITO substrate at a spinning rate of 1400 rpm for 1 min. Then the residual dimethylacetamide solvent was removed under a vacuum oven at 120°C for 4 h. The 120-nm-thick Al electrodes were evaporated onto the PI surface by shadow mask at high vacuum of 2×10^{-3} Pa with a deposition rate of about 1 Å s^{-1}. As shown in Fig. S8, surface morphology of PI films was measured through AFM. The spin-coated PI films provide relatively smooth interface with root-mean-square (RMS) of 1.37, 1.45 and 1.17 nm for DATPP-DSDA, Zn-DATPP-DSDA and Mn-DATPP-DSDA, respectively.

RESULTS AND DISCUSSION

Synthesis and characterization of PIs

Successful synthesis of three PIs (Fig. 1b) were confirmed by FTIR and NMR measurements, as shown in Figs S9–S13. Three porphyrinated PIs are amorphous according to the XRD images (Fig. S14).

DATPP-DSDA: FTIR (KBr, cm^{-1}, Fig. S9): 1782, 1726 (asymmetric and symmetric stretching vibration of C=O), 1365 (C–N stretching), 1148 (–SO_2– stretching), 966 (N–H bending vibration). ^{1}H NMR (d6-DMSO, 400 MHz, ppm, Fig. S11): 8.84 (m, 12H), 8.39 (m, 2H), 8.23 (m, 10H), 7.85 (m, 8H), −2.91 (s, 2H). Number average molecular weight (M_n) and the weight average molecular weight (M_w) are 1.41×10^5 and 1.83×10^5 g mol^{-1}, respectively, with the polydispersity index (D) of 1.30. Elemental analysis: calc. for DATPP-DSDA ($C_{60}H_{34}N_6O_6S$, %): C, 74.52; H, 3.54; N, 8.69; S, 3.32. Found: C, 74.97; H, 3.91; N, 8.26; S, 3.15.

Zn-DATPP-DSDA: FTIR (KBr, cm^{-1}, Fig. S11): 1781, 1726 (asymmetric and symmetric stretching vibration of C=O), 1367 (C–N stretching), 1147 (–SO_2– stretching), 995 (N–Zn bending vibration). ^{1}H NMR (d6-DMSO, 400 MHz, ppm, Fig. S13): 8.85 (m, 12H), 8.35 (m, 2H), 8.17 (m, 10H), 7.87 (m, 2H), 7.81 (m, 6H). M_n and M_w are 1.56×10^5 and 2.01×10^5 g mol^{-1}, respectively, with D of 1.29. Elemental analysis: calc. for Zn-DATPP-DSDA ($C_{60}H_{32}N_6O_6SZn$, %): C, 69.94; H, 3.13; N, 8.16; S, 3.11. Found: C, 70.45; H, 3.64; N, 8.01; S, 2.95.

Mn-DATPP-DSDA: FTIR (KBr, cm^{-1}, Fig. S13): 1781, 1725 (asymmetric and symmetric stretching vibration of C=O), 1365 (C–N stretching), 1150 (–SO_2– stretching), 1009 (N–Mn bending vibration). M_n and M_w are 1.27×10^5 and 1.62×10^5 g mol^{-1}, respectively, with D of 1.27. Elemental analysis: calc. for Mn-DATPP-DSDA ($C_{60}H_{32}N_6O_6SMn$, %): C, 70.66; H, 3.16; N, 8.24; S, 3.14. Found: C, 71.16; H, 3.59; N, 7.95; S, 2.96.

Optical and electrochemical properties

The UV-vis absorption spectra of three porphyrinated PIs are shown in Fig. 1c. The spectra of DATPP-DSDA and Zn-DATPP-DSDA exhibit typical absorption features of porphyrin, such as high intensity Soret band and several Q bands. DATPP-DSDA and Zn-DATPP-DSDA provide a dominant absorption peak at 420 and 428 nm, respectively, which are both corresponding to π-π* transition of porphyrin ring. After the complexation of Zn ion, the electrostatic potential (ESP) maps shown in Fig. 1d demonstrate that the electron distribution at the conjugated backbone of porphyrin ring becomes more delocalized, leading to the facilitated π-π* transition and red shift of max absorption peak. However, for Mn-DATPP-DSDA, the Mn ion exhibits electron-deficient state observed from its ESP map. The typical max absorption peak of

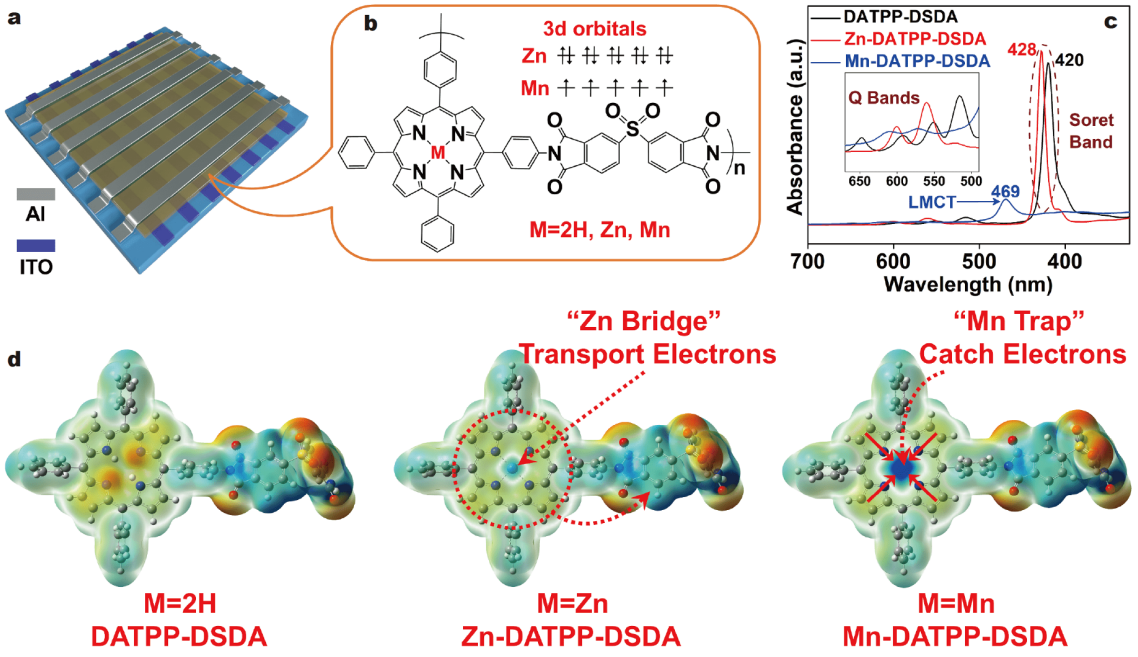

Figure 1 (a) Configuration of the memory device. (b) Chemical structures of porphyrinated PIs. (c) UV-vis spectra of porphyrinated PIs measured in DMF solution. The inserted spectra are the local amplification of Q bands. (d) The electrostatic potential (ESP) maps of porphyrinated PIs.

porphyrin disappears; instead, there is a new comparatively weak max absorption peak at 469 nm, indicating the sharply declined possibility of electron transition. Molecular simulation further demonstrates that the max absorption peak of Mn-DATPP-DSDA is ligand-to-metal charge transfer (LMCT) transition rather than π-π* transition. This change can be explained by that the half-filled 3d orbitals of the Mn ion could attract electrons from the porphyrin ligand, resulting in the distinct features of obvious red shift and weak excited intensity. In addition, the decrease of Q band number of Mn-DATPP-DSDA could also be attributed to the enhanced symmetry of porphyrin structure and orbital degeneracy. Besides, DATPP-DSDA, Zn-DATPP-DSDA and Mn-DATPP-DSDA exhibit the onset absorption edge wavelengths of 667, 623 and 652 nm, respectively. Correspondingly, the energy band gaps (E_g) of the three PIs were estimated to be 1.87, 2.01 and 1.92 eV. Furthermore, the highest occupied molecular orbital (HOMO) and lowest unoccupied molecular orbital (LUMO) energy levels of these three porphyrinated PIs were calculated based on CV measurement (Table 1). As shown in Fig. S15, for DATPP-DSDA and Zn-DATPP-DSDA, the oxidation peaks during the positive sweep of 0 to 2 V are considered as the oxidation process of porphyrin macrocycle. Noticeably, during the sweep from 2 to 0 V, the obvious reduction behavior of Zn-DATPP-DSDA indicates its quasi-reversible p-doping feature (Fig. S15) which could verify the role of the Zn ion in regulating the charge transfer process and imply its potential volatility of memory device. For Mn-DATPP-DSDA, the onset oxidation potential is obviously reduced compared with the other two PIs. It is considered that the oxidation peak also involves the oxidation of central Mn ion. The obviously reduced onset oxidation potential is due to the increased α HOMO level, as shown in Fig. S16. All above-mentioned results clearly imply that the various central metal ions with distinct 3d orbitals could determine the electron excitation processes which provides the possibility of controlling the CTC formation of porphyrinated PI.

Molecular simulation

To better understand the memory mechanism and charge transfer processes, molecular simulation on basic units for porphyrinated PIs was carried out with Gaussian 09 package. The optimized geometries and frontier orbitals at ground state were calculated at DFT/b3lyp/TZVP level, as shown in Fig. S16. The little difference of these calculated results demonstrates that the alteration on electronic structure of PIs at ground state is limited after complexation of various metal ions. As shown in Fig. S17, the dihedral angle between the electron donor and ac-

Table 1 Optical and electrochemical properties of porphyrinated PIs

	UV-vis (nm)		ε^{a} of Soret band (10^5 L mol^{-1} cm^{-1})	E_{ox}(onset) (V) (from CV)	E_g^{b} (eV)	HOMO^{c} (eV)	LUMO^{d} (eV)
	λ_{max}	λ_{edge}					
DATPP-DSDA	420	667	2.3	0.79	1.86	−5.21	−3.35
Zn-DATPP-DSDA	428	623	2.5	0.83	2.01	−5.25	−3.24
Mn-DATPP-DSDA	469	652	0.7	0.65	1.92	−5.07	−3.15

a) Calculated from the equation: $A= \varepsilon cl$, where A, ε, c and l are the absorbance, molar extinction coefficient, concentration and thickness of cuvette, respectively. b) Calculated from the UV/vis absorption edge wavelength (λ_{edge}) by using the Planck equation $E_g = 1240/\lambda_{edge}$. c) The HOMO energy levels were calculated from CV onset oxidation potential (E_{ox}(onset)) and were referenced to ferrocene (4.8 eV below the vacuum level). $E_{ferrocene}$ is determined to be 0.38 V *vs.* Ag/AgCl. HOMO = −[(E_{ox}(onset) − $E_{ferrocene}$) + 4.8] (eV). d) Determined from the equation: LUMO = E_g + HOMO.

ceptor is almost the same for the three porphyrinated PIs, excluding the steric effect on memory performance. Considering the variation of UV-vis absorption spectra, the information of excited states was calculated and the corresponding UV-vis absorption spectra were fitted at TDDFT/cam-b3lyp/TZVP level. And properties of excited states (colorful vertical lines) are provided in the spectra, including the absorption wavelength and oscillator strength. Q, M and S represent Q bands, max absorption peak and shoulder peak, respectively. Taking M1 in absorption spectrum of DATPP-DSDA as an example (Fig. 2a), M1 represents the first excited state contributing to the max absorption peak of DATPP-DSDA. The UV-vis absorption spectra could provide both curve shape and characteristics similar to experimental results, including the decrease of number of Q bands (analyzed in the Supplementary information, Fig. S18 and Tables S1, S2), narrower max absorption peak and weaker absorption intensity of shoulder peak for Zn-DATPP-DSDA (Fig. 2b) as well as the distinct absorption spectrum for Mn-DATPP-DSDA (Fig. 2c), which could verify the rational choice of functional and basis set. The concerned charge transfer excitations (CTE) appear in the regions of max absorption peaks, and thus the enlargement spectra of max absorption peaks are also provided. The CTE of DATPP-DSDA possesses oscillator strength of 0.0291 (Fig. 2d). Unexpectedly, this value for Zn-DATPP-DSDA is 0.4094 (Fig. 2e), which is extraordinarily high for CTE. However, with the insertion of Mn ions, none of excited states exhibit the characteristic of charge transfer (Fig. 2f). The entirely opposite effects of these two metal ions on the CTE processes may further control the memory performances of porphyrinated PIs.

To deeply investigate the significant roles of metal ions in the charge transfer processes, the contributions of molecular orbital transition and charge density difference in whole space (blue and purple isosurfaces represent the hole and electron distributions, respectively) were further studied with Multiwfn package [44], as shown in Table 2. What's more, all properties of excited states in the full wavelength range for three PIs are listed in Tables S3–S5. It is found that for both DATPP-DSDA and Zn-DATPP-DSDA, the main molecular orbital transition is from HOMO to LUMO. Furthermore, for Zn-DATPP-DSDA, there is another dominant excited state at 364.77 nm with high oscillator strength of 1.3774, exhibiting the characteristic of charge transfer. These two charge transfer excitations in Zn-DATPP-DSDA demonstrate that the Zn ion plays a "Zn bridge" role in transporting electrons, in other words, the Zn ion could construct an efficient channel to transport electrons from D to A moieties under an external field directly. This could be explained by that the Zn ion with fully filled 3d orbitals facilitates the formation of π feed-back bonding which could increase the electronic density of porphyrin as electron donor and may further affect the charge transfer process. However, for Mn-DATPP-DSDA, half-filled 3d orbitals of the Mn ion could accommodate excited electrons from surrounding porphyrin ring and affect the inherent excitations of porphyrin. Therefore, all involved excited states possess similar charge distribution, that is, holes mainly distribute on porphyrin moiety and electrons mainly distribute on the central Mn ion and porphyrin moiety (Table S5). It is considered that the Mn ion plays a "Mn trap" role, resulting in the interrupted CTE from D to A and atypical absorption curve of Mn-DATPP-DSDA. It is evident that the central metal ions play distinct roles in regulating the charge transfer process, which is consistent with experimental results from UV-vis absorption spectra and CVs.

Memory effects and memory mechanism

The electrical memory performances of the porphyrinated PIs were investigated by the current-voltage (*I-V*) curves based on Al/PIs/ITO sandwiched devices. As shown in Fig. 3a, for DATPP-DSDA, the device is initially

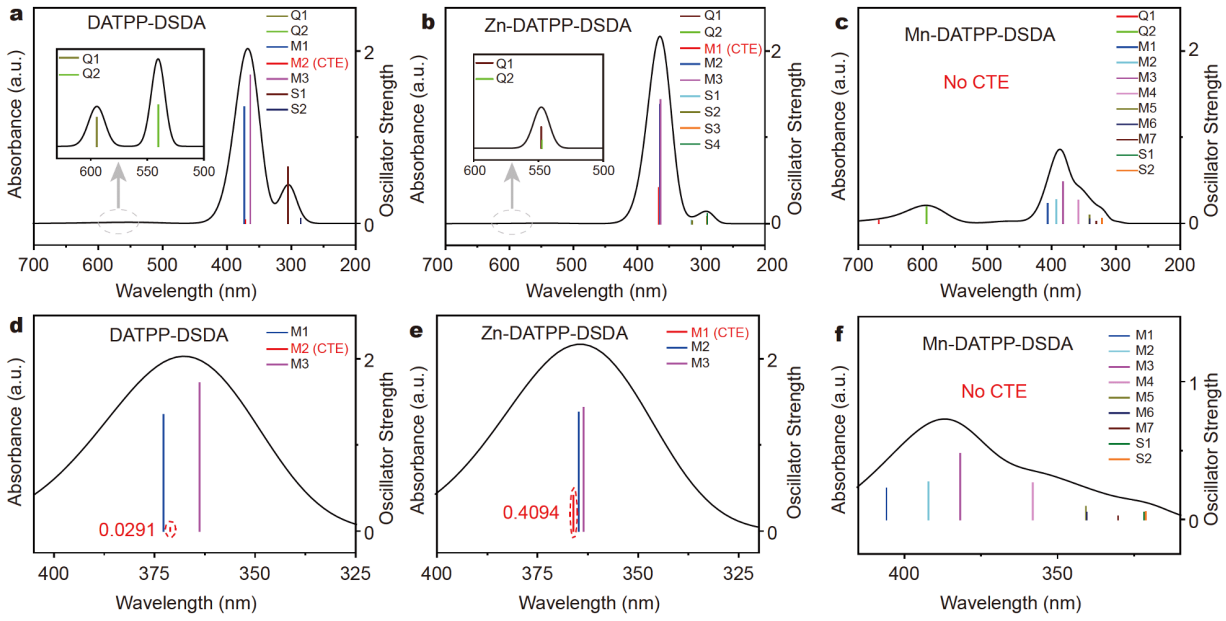

Figure 2 Calculated UV-vis absorption spectra and the calculated max absorption peaks and involved excited states of (a, d) DATPP-DSDA, (b, e) Zn-DATPP-DSDA and (c, f) Mn-DATPP-DSDA.

Table 2 Properties of CTE for porphyrinated PIs

Polyimide	Excitation	Wavelength	Oscillator strength	Difference	Contribution of MO transition (%)
DATPP-DSDA	M2	371.08	0.0291	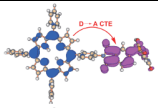	HOMO→LUMO (78.09) HOMO→LUMO+1 (17.31)
Zn-DATPP-DSDA	M1	366.07	0.4094	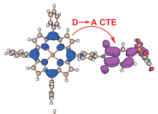	HOMO→LUMO (62.96) HOMO→LUMO+1 (13.55)
	M2	364.77	1.3774	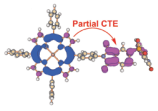	HOMO-1→LUMO+3 (41.28) HOMO→LUMO+2 (35.90) HOMO→LUMO (16.05)
Mn-DATPP-DSDA			No charge transfer states		

at the low conductivity state (OFF) with a current around 10^{-7} A, and then a sharp increased current level at 10^{-3} A is observed with a bias voltage of 1.4 V, indicating the transition of the device from the low conductivity (OFF) to high conductivity (ON). And then, the device could maintain its high conductivity even after setting negative sweep or removing the power for minutes, which exhibits the WORM characteristic of DATPP-DSDA with the threshold voltage of 1.4 V and ON/OFF ratio of 10^4. By introducing a Zn ion into the porphyrin ring, the ON state of Zn-DATPP-DSDA-based devices could be switched to OFF state after removing the voltage field for 7 min and then returned to ON state by subsequent voltage sweep, which indicates that its memory performance is triggered to SRAM with the threshold voltage of 1.4 V and ON/OFF ratio of 10^4 (Fig. 3b). It is considered that the inserted Zn ion just establishes a convenient bridge for the transfer process of electrons at D moiety and does not affect the amount of charge transfer, which leads to the same hole and electron distributions as well as the almost identical ON/OFF ratios of DATPP-DSDA and Zn-DATPP-DSDA. The HOMO and LUMO levels as

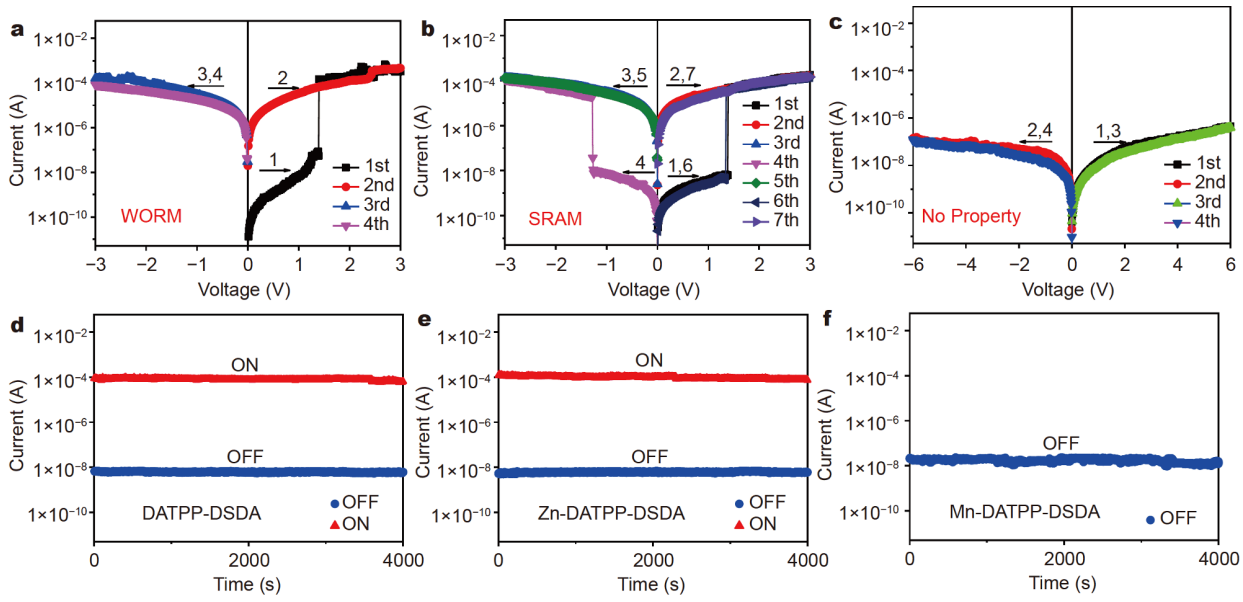

Figure 3 *I-V* characteristic and retention performances of (a, d) DATPP-DSDA, (b, e) Zn-DATPP-DSDA and (c, f) Mn-DATPP-DSDA.

well as their energy barrier with electrode pairs dominate the charge transfer and hole injection processes. And the inserted Zn ion brings limited influence on these values, so there is little difference in the threshold voltages of the two PIs. Expectedly, Mn-DATPP-DSDA-based devices show no electrical bi-stable states (Fig. 3c). No sharp increase in current appears regardless of any positive or negative voltage sweeps, demonstrating that the Mn-DATPPP-DSDA-based devices do not possess any memory performance. To evaluate the stability of the memory devices, the retention characteristics of the devices using DATPP-DSDA and Zn-DATPP-DSDA as the active layers were measured, respectively. As shown in Fig. 3d–f, no degradation of current is observed during the test with a read voltage of 2 V for 4000 s, reflecting the two kinds of devices provide good stability for both ON and OFF states. Thus, it is experimentally proved that Zn and Mn ions could play various roles in tailoring memory behaviors of porphyrinated PIs.

According to the results of molecular simulation, Zn and Mn ions produce distinct effect on CTE of porphyrinated PIs and different memory mechanisms are provided. For DATPP-DSDA (Fig. 4a), when the external electrical field reaches the threshold voltage, the electrons at HOMO gain adequate energy and transit to LUMO+2 which both possess much overlapping with HOMO, followed by relaxation to LUMO, leading to the formation of conductive CTC. And charge transfer could also occur *via* the electrons at HOMO being directly excited to LUMO at low probability. Then charge carriers are extensively injected along the CTC, consequently turning the device to a high-conductivity state (ON state). Sulfonyl and carbonyl groups endow the DSDA moiety with strong electron-catching ability which could maintain the charge transfer state, producing the DATPP-DSDA device with the nonvolatile WORM performance. For Zn-DATPP-DSDA (Fig. 4b), CTE with remarkably high oscillator strength provides unique memory mechanism. At the threshold voltage, electrons at HOMO readily cross the convenient "Zn bridge" and reach LUMO at DSDA moiety, leading to the formation of CTC and switching the memory device to ON state. After removing the external field for minutes, the excited electrons would return to low-energy HOMO *via* "Zn bridge", resulting in the relaxation of CTC and turning memory device to low-conductivity OFF state. Thus the Zn-DATPP-DSDA-based devices exhibit volatile SRAM behavior due to the "Zn bridge" effect. For Mn-DATPP-DSDA (Fig. 4c), the Mn ion with specific half-filled 3d orbitals plays a "Mn trap" role, completely different from Zn ion. Under external voltage field, electrons at porphyrin moiety would be caught by central "Mn trap" rather than be excited to LUMO at DSDA moiety, failing to form CTC. The "Mn trap" effect makes the Mn-DATPP-DSDA-based devices exhibit no memory behaviors.

CONCLUSIONS

DATPP-DSDA, Zn-DATPP-DSDA and Mn-DATPP-

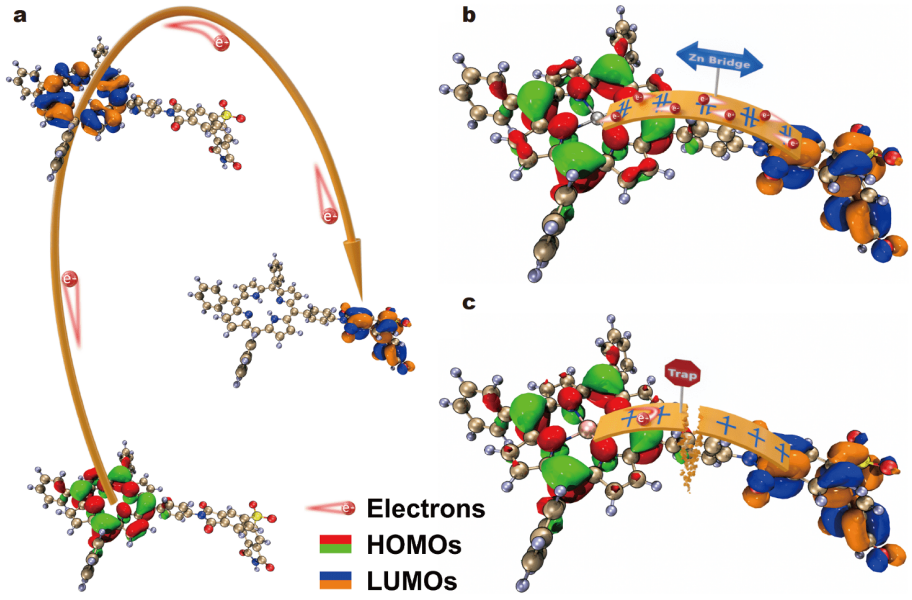

Figure 4 Memory mechanism of the devices based on (a) DATPP-DSDA, (b) Zn-DATPP-DSDA and (c) Mn-DATPP-DSDA.

DSDA were designed and synthesized as active layers for memory devices. Central various metal ions with different features of 3d orbitals could effectively regulate the electronic structures and charge transfer processes of porphyrinated PIs, leading to the distinct optoelectronic and electrochemical performances of the three porphyrinated PIs. Molecular simulation demonstrates that Zn-DATPP-DSDA possesses CTE with extraordinarily increased oscillator strength compared with DATPP-DSDA, but there is no any CTE for Mn-DATPP-DSDA. Further analysis of the charge distribution of excited states indicates that the Zn ion could establish an efficient bridge for electrons at HOMO being excited to LUMO, while the Mn ion plays a trap role in catching electrons from surrounding porphyrin moiety. Current-voltage characteristics indicate that DATPP-DSDA exhibits non-volatile WORM performance, Zn-DATPP-DSDA possesses volatile SRAM behavior due to the "Zn bridge" effect, and no electrical bi-stable states for Mn-DATPP-DSDA caused by the "Mn trap" effect. This study could certify the feasibility of controlling memory performances *via* varying the central metal ions in porphyrinated PIs and provide the guideline for researchers to obtain desirable optoelectronic performance of organic materials containing metalloporphyrins.

Received 4 September 2020; accepted 11 November 2020; published online 1 February 2021

1 Ling QD, Liaw DJ, Teo EYH, *et al.* Polymer memories: Bistable electrical switching and device performance. Polymer, 2007, 48: 5182–5201
2 Ling QD, Liaw DJ, Zhu C, *et al.* Polymer electronic memories: Materials, devices and mechanisms. Prog Polym Sci, 2008, 33: 917–978
3 Heremans P, Gelinck GH, Muller R, *et al.* Polymer and organic nonvolatile memory devices. Chem Mater, 2011, 23: 341–358
4 Chen Y, Liu G, Wang C, *et al.* Polymer memristor for information storage and neuromorphic applications. Mater Horiz, 2014, 1: 489–506
5 Kurosawa T, Higashihara T, Ueda M. Polyimide memory: A pithy guideline for future applications. Polym Chem, 2013, 4: 16–30
6 Yang Y, Xia J, Ding Z, *et al.* Synthesis and resistive switching characteristics of polyimides derived from 2,7-aryl substituents tetraphenyl fluorene diamines. Eur Polym J, 2018, 108: 85–97
7 Khan QU, Tian G, Bao L, *et al.* Highly uniform supramolecular nano-films derived from carbazole-containing perylene diimide *via* surface-supported self-assembly and their electrically bistable memory behavior. New J Chem, 2018, 42: 11506–11515
8 Kim Y, Song S, Liaw DJ, *et al.* Digital memory characteristics of aromatic polyimides based on pyridine and its derivatives. ACS Omega, 2018, 3: 13036–13044
9 Yen HJ, Chen CJ, Wu JH, *et al.* High performance polymers and their PCBM hybrids for memory device application. Polym Chem, 2015, 6: 7464–7469
10 Chen CJ, Yen HJ, Chen WC, *et al.* Resistive switching non-volatile and volatile memory behavior of aromatic polyimides with various electron-withdrawing moieties. J Mater Chem, 2012, 22: 14085
11 Tian G, Wu D, Qi S, *et al.* Dynamic random access memory effect and memory device derived from a functional polyimide containing electron donor-acceptor pairs in the main chain. Macromol Rapid Commun, 2011, 32: 384–389
12 Ye H, Tian G, Shi L, *et al.* Polymer memory devices with widely tunable memory characteristics based on functional copoly-

naphthalimides bearing varied fluorene and triphenylamine moieties. Eur Polym J, 2015, 63: 45–57
13 Lin LC, Yen HJ, Chen CJ, *et al.* Novel triarylamine-based polybenzoxazines with a donor–acceptor system for polymeric memory devices. Chem Commun, 2014, 50: 13917–13920
14 Liu Y, Zhang Y, Lan Q, *et al.* High-performance functional polyimides containing rigid nonplanar conjugated triphenylethylene moieties. Chem Mater, 2012, 24: 1212–1222
15 Shi L, Ye H, Liu W, *et al.* Tuning the electrical memory characteristics from worm to flash by α- and β-substitution of the electron-donating naphthylamine moieties in functional polyimides. J Mater Chem C, 2013, 1: 7387–7399
16 Yang Y, Xia JC, Zheng Y, *et al.* Synthesis and non-volatile electrical memory characteristics of triphenylamine-based polyimides with flexibility segments. New J Chem, 2018, 42: 19008–19019
17 Kurosawa T, Yu AD, Higashihara T, *et al.* Inducing a high twisted conformation in the polyimide structure by bulky donor moieties for the development of non-volatile memory. Eur Polym J, 2013, 49: 3377–3386
18 Yang Y, Ding Z, Xia J, *et al.* Nonvolatile write-once read-many-times memory behaviors of polyimides containing tetraphenyl fluorene core and the pendant triphenylamine or carbazole moieties. J Polym Sci Part A-Polym Chem, 2018, 56: 1630–1644
19 Yu HC, Kim MY, Lee JS, *et al.* Fully transparent nonvolatile resistive polymer memory. J Polym Sci Part A-Polym Chem, 2016, 54: 918–925
20 Yu AD, Kurosawa T, Lai YC, *et al.* Flexible polymer memory devices derived from triphenylamine–pyrene containing donor–acceptor polyimides. J Mater Chem, 2012, 22: 20754
21 Choi TL, Lee KH, Joo WJ, *et al.* Synthesis and nonvolatile memory behavior of redox-active conjugated polymer-containing ferrocene. J Am Chem Soc, 2007, 129: 9842–9843
22 Xiang J, Wang TK, Zhao Q, *et al.* Ferrocene-containing poly (fluorenylethynylene)s for nonvolatile resistive memory devices. J Mater Chem C, 2016, 4: 921–928
23 Hao R, Jia N, Tian G, *et al.* Flash memory effects and devices based on functional polyimides bearing pendent ferrocene group. Mater Des, 2018, 139: 298–303
24 Goswami S, Matula AJ, Rath SP, *et al.* Robust resistive memory devices using solution-processable metal-coordinated azo aromatics. Nat Mater, 2017, 16: 1216–1224
25 Liu SJ, Lin ZH, Zhao Q, *et al.* Flash-memory effect for polyfluorenes with on-chain iridium(III) complexes. Adv Funct Mater, 2011, 21: 979–985
26 Cheng XF, Shi EB, Hou X, *et al.* 1d π-d conjugated coordination polymers for multilevel memory of long-term and high-temperature stability. Adv Electron Mater, 2017, 3: 1700107
27 Choi S, Hong SH, Cho SH, *et al.* High-performance programmable memory devices based on hyperbranched copper phthalocyanine polymer thin films. Adv Mater, 2008, 20: 1766–1771
28 Koo B, Baek H, Cho J. Control over memory performance of layer-by-layer assembled metal phthalocyanine multilayers *via* molecular-level manipulation. Chem Mater, 2012, 24: 1091–1099
29 Suslick KS, Rakow NA, Kosal ME, *et al.* The materials chemistry of porphyrins and metalloporphyrins. J Porphyrins Phthalocyanines, 2000, 04: 407–413
30 Ji JM, Kim SH, Zhou H, *et al.* D–π–A-structured porphyrins with extended auxiliary π-spacers for highly efficient dye-sensitized solar cells. ACS Appl Mater Interfaces, 2019, 11: 24067–24077
31 Sun Y, Gao H, Zhang Y, *et al.* An efficient ternary organic solar cell with a porphyrin based small molecule donor and two fullerene acceptors. Chin J Org Chem, 2018, 38: 228
32 Tanguy L, Malhotra P, Singh SP, *et al.* A 9.16% power conversion efficiency organic solar cell with a porphyrin conjugated polymer using a nonfullerene acceptor. ACS Appl Mater Interfaces, 2019, 11: 28078–28087
33 Graham KR, Yang Y, Sommer JR, *et al.* Extended conjugation platinum(II) porphyrins for use in near-infrared emitting organic light emitting diodes. Chem Mater, 2011, 23: 5305–5312
34 Janghouri M, Adineh M. Color optimization of red organic light emitting diodes (OLEDs) through dihydroxyphenyl-substituted zinc porphyrins emitters. J Photochem Photobiol A-Chem, 2017, 341: 31–38
35 Verykios A, Papadakis M, Soultati A, *et al.* Functionalized zinc porphyrins with various peripheral groups for interfacial electron injection barrier control in organic light emitting diodes. ACS Omega, 2018, 3: 10008–10018
36 Mesbahi E, Safari N, Gheidi M. Investigation of axial ligand effects on catalytic activity of manganese porphyrin, evidence for the importance of hydrogen bonding in cytochrome-p450 model reactions. J Porphyrins Phthalocyanines, 2014, 18: 354–365
37 da Silva VS, Teixeira LI, do Nascimento E, *et al.* New manganese porphyrin as biomimetic catalyst of cyclohexane oxidation: Effect of water or imidazole as additives. Appl Catal A-General, 2014, 469: 124–131
38 Zanardi FB, Barbosa IA, de Sousa Filho PC, *et al.* Manganese porphyrin functionalized on Fe_3O_4@nSiO_2@MCM-41 magnetic composite: Structural characterization and catalytic activity as cytochrome P450 model. Microporous Mesoporous Mater, 2016, 219: 161–171
39 Hassan SSM, Kelany AE, Al-Mehrezi SS. Novel polymeric membrane sensors based on Mn(III) porphyrin and Co(II) phthalocyanine ionophores for batch and flow injection determination of azide. Electroanalysis, 2008, 20: 438–443
40 Saraswathyamma B, Pajak M, Radecki J, *et al.* PVC supported liquid membrane and carbon paste potentiometric sensors incorporating a Mn(III)-porphyrin for the direct determination of undissociated paracetamol. Electroanalysis, 2008, 20: 2009–2015
41 Shao M, Xu X, Han J, *et al.* Magnetic-field-assisted assembly of layered double hydroxide/metal porphyrin ultrathin films and their application for glucose sensors. Langmuir, 2011, 27: 8233–8240
42 Tsai CL, Sudhir K Reddy K, Yeh CY, *et al.* Zinc and linkage effects of novel porphyrin-containing polyimides on resistor memory behaviors. RSC Adv, 2016, 6: 88531–88537
43 Tsai MC, Wang CL, Lin CY, *et al.* A novel porphyrin-containing polyimide for memory devices. Polym Chem, 2016, 7: 2780–2784
44 Lu T, Chen F. Multiwfn: A multifunctional wavefunction analyzer. J Comput Chem, 2012, 33: 580–592

Acknowledgements The authors sincerely appreciate the financial support from the National Natural Science Foundation of China (51673017 and 62004138), Beijing National Laboratory for Molecular Sciences (BNLMS202006), the Fundamental Research Funds for the Central Universities (XK1802-2), the National Key Basic Research Program of China (973 program, 2014CB643604), and the Natural Science Foundation for Distinguished Young Scholars of Jiangsu Province (BK20140006).

Author contributions Guo J, Zhang Y, Ji D and Qi S conceived and designed the experiments. Guo J and Zhang Y performed the experi-

ments and molecular simulations. Guo J, Zhang Y, Wu D, Ji D, Qi S and Hu W discussed the results and co-wrote the manuscript.

Conflict of interest The authors declare no conflict of interest.

Supplementary information Experimental details and supporting data are available in the online version of the paper.

Jiacong Guo received his BEng degree from Nanjing Tech University in 2016. He is now a PhD student at Beijing University of Chemical Technology. His research interests are polyimide memory materials.

Deyang Ji is currently a Professor at the Institute of Molecular Aggregation Science, Tianjin University. He received his BSc degree from Ocean University of China in 2009. He received his PhD degree from the Institute of Chemistry, Chinese Academy of Sciences, in 2014 under the supervision of Prof. Wenping Hu. Then, he joined the University of Münster, Germany, as a postdoc fellow in the group of Prof. Harald Fuchs. His research interest focuses on organic optoelectronics.

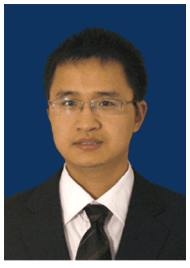

Shengli Qi is currently a Professor at the School of Materials Science and Engineering, Beijing University of Chemical Technology, China. He received his PhD degree from Beijing University of Chemical Technology in 2008. Then he worked in Nagoya University as a postdoctoral fellow of Japan Society for the Promotion of Sciences in 2009–2011. His research focuses on high-performance and functional polyimide and its applications in flexible display, information storage and secondary energy systems.

存储器件中由金属离子3d轨道电子排布控制的电荷转移过程

郭家聪[1], 张焱坤[1], 田国峰[1], 纪德洋[2,3*], 齐胜利[1,4*], 武德珍[1,4], 胡文平[5]

摘要 具有电双稳态的功能性聚合物材料因其纳米尺寸的存储位点、3D可堆叠性和固有柔性等优点，在高密度数据存储领域展现出巨大的应用潜力. 具有电子给体-受体结构的聚酰亚胺在电场下可以形成电荷转移络合物，使其可以作为存储材料. 本文合成了三种卟啉基聚酰亚胺DATPP-DSDA、Zn-DATPP-DSDA和Mn-DATPP-DSDA用于信息存储. 研究发现金属离子的不同3d轨道电子排布对于聚酰亚胺的存储行为有决定性的影响. 其中，DATPP-DSDA展现出非易失性WORM存储行为，Zn-DATPP-DSDA展现出易失性SRAM存储行为，而Mn-DATPP-DSDA不具有存储性能. 通过分析轨道跃迁贡献和电荷转移激发态的空穴-电子分布，研究了不同金属离子调节存储行为类型的作用. 分子模拟结果表明锌离子起到一个“桥”的作用，可以促使电子从电子给体转移到电子受体部分，而锰离子起到一个“阱”的作用来阻止这一过程. 对于卟啉基聚酰亚胺，这一研究证明了通过改变中心金属离子来调节存储行为的策略是可行的，并且提出了不同金属离子调节电荷转移过程的不同作用.